Strain-Engineering Deformable Amorphous Metal Electrodes: Insights from Optical Imaging

Abdarahmane Thiam,[†] Christophe Rousselot,[‡] Yves Gaillard,[†] Marina Raschetti,[†] Marion Vieira,[†] Nicolas Martin,[†] Frédéric Kanoufi,[¶] and Fabien Amiot[*,†]

[†]*Université Marie et Louis Pasteur, CNRS, institut FEMTO-ST, 25000 Besançon, France*

[‡]*Université Marie et Louis Pasteur, CNRS, institut FEMTO-ST, 25200 Montbéliard, France*

[¶]*ITODYS, Université de Paris, CNRS, 13 rue Antoine de Baif, 75013 Paris*

E-mail: fabien.amiot@femto-st.fr

Phone: +33 (0)381666014

Abstract

Amorphous electrodes and amorphous/crystalline interfaces are garnering increasing interest in water-splitting applications. In these systems, mechanical strain—particularly at amorphous/crystalline interfaces—plays a critical role in influencing overall performance. A deeper understanding of how mechanical strain affects the catalytic activity of amorphous metals is therefore essential for optimizing their functionality. However, the impact of mechanical strain on the electrocatalytic behavior of amorphous metals has received surprisingly little attention in the literature. An optical imaging method is presented to spatially resolve local pH changes at electrode surfaces during water splitting, thereby enabling the visualization of the local hydrogen production rate. This technique is applied to investigate the electrocatalytic behavior of deformable electrodes composed of amorphous metals, which allow for exceptionally large strains and thus significant strain-engineering capabilities. The results reveal spatial non-uniformity in hydrogen production across planar electrodes, underscoring the necessity of spatially resolved measurements in electrocatalysis at small scales. The study further demonstrates the critical role of mechanical strain in modulating electrocatalytic performance, establishing this approach as a powerful tool for optimizing strain-engineered electrode materials in advanced energy conversion systems.

Keywords

amorphous electrodes, pH imaging, water splitting, electrocatalysis, strain-engineering

This document is distributed under a Creative Commons Attribution — 4.0 International licence CC BY. https://creativecommons.org/licenses/by/4.0/

1 Introduction

Hydrogen is currently obtained primarily by hydrocarbon steam reforming, which produces large quantities of CO_2. Because of the rising concern about greenhouse gas emissions, the widespread use of hydrogen as an energy carrier requires the development of a carbon-free production chain. In case it makes use of renewable electricity sources, hydrogen production by electrolysis may be the key to triggering the expansion of this promising sector. However, only a few percent of the total hydrogen production comes today from water electrolysis, mainly because of its cost, which is about four times higher than that of hydrogen obtained by steam reforming. Electrolysis requires an electrocatalyst, typically platinum, which is rare and expensive. Electrolytic production of H_2 is thus hindered by its dependence on platinum. It is therefore crucial, to minimize the cost and energy losses, to avoid materials like platinum as much as possible. It has already been demonstrated, through density functional theory (DFT) computation[1,2] or experiments at various scales.[3–7] This suggests that elastic strains can modulate the electrocatalytic activity of metals, so that more abundant materials could be strained to achieve electrocatalytic activity comparable to that platinum.[8] The widely accepted model for describing this strain effect is the d-band model.[1] However, bridging the atomic scale simulations with the electrolyzer's performances remains a challenge whatever the considered material, and this requires experimental approaches at intermediate scales.

Amorphous materials are widely recognized for their exceptional catalytic potential,[9] particularly in water-splitting technologies. Their high activity and broad chemical versatility make them ideal candidates for advancing sustainable energy solutions.[10] Moreover, their catalytic performance can be systematically tuned through various strategies,[11] with strain-engineering emerging as a promising approach[12] due to their extended elastic regime.

The role of amorphous metals as electrodes is further underscored by the growing interest in amorphous/crystalline interfaces. These interfaces, which can be generated through cost-effective processes,[13–16] synergistically combine the high conductivity of crystalline phases with the superior catalytic activity of amorphous phases. The elastic strains required to

accommodate such interfaces also enhance overall catalytic performance.[17] Consequently, a deeper understanding of how mechanical strain influences the catalytic activity of amorphous metals is essential for optimizing their functionality.

Despite these advantages, very few studies have explored the impact of mechanical strain on the electrocatalytic behavior of amorphous metals. This gap is particularly notable given their extensive elastic regime, which offers significant opportunities for strain-engineering and performance enhancement. The question of the optimal mechanical state remains open, and we propose an experimental approach based on an imaging technique to monitor in-situ and in-operando the local hydrogen production rate. It is applied to monitor the local hydrogen production rate on microfabricated deformable electrodes made out of an amorphous metal thin film.

The findings first reveal that hydrogen production is spatially non-uniform across the electrodes, underscoring the necessity of spatially resolved experimental approaches for small-scale investigations. Furthermore, the critical role of mechanical strain in the electrocatalytic activity of the considered amorphous material is clearly demonstrated, with compression slightly increasing the production rate. This paves the way for the optimization of strain-engineered amorphous electrode materials. Additionally, the proposed imaging technique is expected to serve as a valuable tool for both electrode monitoring and fundamental research.

2 Experimental sections

2.1 Imaging

All objects in this study have been imaged using the same reflection microscope. The sample was illuminated using a stabilized white lamp with interference filters to select a monochromatic illumination in the visible range (490 and 700 nm). All the images in this study were obtained with an Olympus UMPLFLN-20XW water immersion objective (NA=0.5), with a drop of the considered solution between the objective front and the sample. The images

were recorded using a PhotonFocus MV-D1024E-160-CL camera at a 4 Hz frequency, so that the pixel dimension is about 140 nm. The sample's surface was aligned orthogonal to the optical axis of the microscope by using a Mirau objective, before any measurement. The surface reflectivity R is defined as the ratio of the intensity recorded on the camera I during the experiment to the same intensity recorded prior to the experiment I_0.

2.2 Materials

The gold films used for validation purpose were obtained by evaporating a 100 nm thick gold layer on top of a 5 nm thick Cr adhesion layer onto an as-received silicon (100) wafer.

Starting from a silicon (100) wafer, a $Zr_{65}Ni_{35}$ layer was sputtered onto the surface from a composite target and further structured by lift-off. Suspended structures were subsequently obtained by etching the underlying silicon (TMAH 10 %, 80°C), resulting in uniform matrices of $80 \times 15 \times 0.5\mu\text{m}^3$ cantilevers. 500 nm thick $Zr_{65}Ni_{35}$ films were also deposited onto a (100) silicon wafer for calibration purpose. The composition of the films was verified by EDS measurements. X-ray diffraction under grazing incidence was further used to confirm the amorphous structure of the film. Its resistivity was evaluated by a four point probe measurement.

2.3 Mechanical properties of the metallic glass

Its elastic behavior was further characterized by nano-indentation (UNHT1, Anton Paar). A Berkovich indenter, whose shape area function was calibrated using fused silica, was used. Indentations were performed using constant strain rate loading up to a load of 40mN. Continuous stiffness measurement (CSM) was used in order to assess to hardness and elastic modulus during the whole loading segment. Hardness and modulus were calculated using the Oliver and Pharr method[18] assuming a Poisson's coefficient of 0.3. In order to estimate the elastic range, a sphero-conical indenter (radius : 7.9μm) was used. The transition between elastic and elasto-plastic behaviour seems to be characterised for such material by a

displacement burst, also called pop-in[19,20] (see SI). This was confirmed by the observation of the residual imprint after indentation by atomic force microscopy (AFM). No residual imprint could be observed for nanoindentation performed below the pop-in, whereas residual imprints in the nanometer range were distinguished for indentation performed at higher loads. In order to assess the random nature of the pop-in, conical indentations in CSM mode were repeated 100 times and the mean contact pressure (P) at the displacement burst were extracted.

2.4 Electrochemistry

After plasma cleaning, all these objects (gold films, $Zr_{65}Ni_{35}$ films and $Zr_{65}Ni_{35}$ micro-cantilevers) were used as working electrodes, together with a platinum wire counter-electrode and an acidic (pH 3.1 or pH 4.3) KCl 0.1 M solution possibly containing lanthanum hydroxide at 1 mM. The electrode surface area was defined using an adhesive, 43 μm thick Kapton film in which a 0.5 mm hole was drilled. The electrochemical behavior was studied by performing chronopotentiometric measurements for varied charge steps (varied cathodic current values) during 50 s. The current was then set to 0 μA (self-discharge or recovery step). During these experiments, images of the surface and of the cantilever were recorded under constant illumination, at either 490 or 700 nm. This allowed monitoring the reflectivity of the surface at the early stage of hydrogen production.

2.5 Mechanical loading

A glass capillary was also used to impose an initial deformation to the cantilever, so that these chrono-potentiometric and reflectivity measurements were performed for cantilevers with varied external mechanical loadings. This was achieved by placing the capillary tip in contact with the cantilever's surface, either on the top or the bottom side. The contact point was detected through the induced cantilever apparent reflectivity change. The capillary was subsequently displaced along the normal to the surface thanks to a P611-1S piezo actuator with a E-665.XR servo-controller (PI instruments). Because of the large elastic range of

the materials, only the depth of field of the used objective lens limited the maximum tip displacement.

3 Results and discussion

3.1 Reflectivity-based imaging mechanism

We focused on the hydrogen evolution reaction (HER) in acidic media. Gold surfaces were first used as electrodes to validate that the surface reflectivity changes during hydrogen production result from the lanthanum hydroxide precipitation (see Figure 1). This allows monitoring the surface reflectivity R in-operando. As illustrated in Figure 1, the electrode's

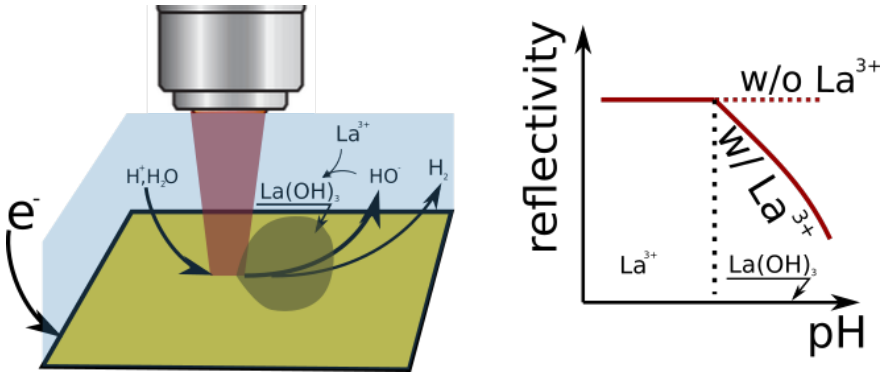


Figure 1: Schematic view of the reported experiments.

surface is constantly illuminated and the reflected light is collected during the hydrogen production. In case there is no lanthanum hydroxide in the solution, the surface reflectivity R (under illumination at 490 nm) slightly increases with the charge of the electrode and quickly saturates (Figure 2a), probably as a result of the diffusion layers settlement (see SI). When lanthanum hydroxide is added, the same behavior is initially observed, and the reflectivity starts to significantly decrease at a certain time, denoted t_{pH}, which depends on the current density. This observation validates the role of lanthanum hydroxide as an optical probe.

A detailed modeling of the diffusion at the electrode surface is described in the Sup-

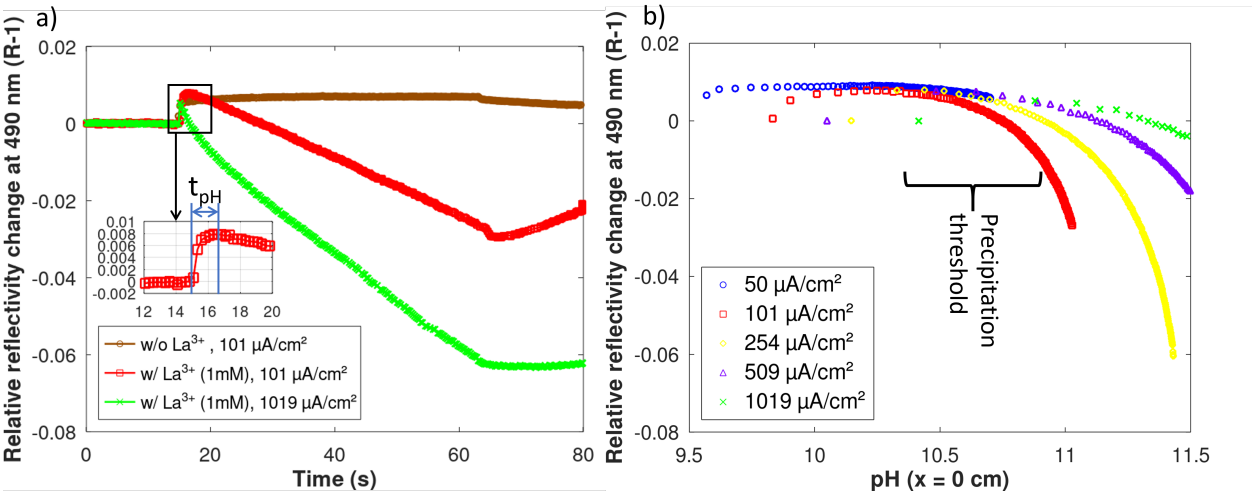


Figure 2: a) Relative reflectivity change of the gold electrode at 490 nm as a function of time in solutions with and without lanthanum hydroxide in the electrolyte, for two different current densities. Inset : Early reflectivity changes, with the definition of time t_{pH} at which precipitation starts. b) Relative reflectivity change at 490 nm as a function of the computed pH at the gold electrode surface in a lanthanum hydroxide containing solution at pH=4.3.

plementary Information (SI). It is based on the exact solution of the diffusion problems associated with both the considered reactions. The model aims to predict the time at which the lanthanum hydroxide layer starts to form, modifying the interfacial reflectivity. It should be noted that for the sake of simplicity, it is chosen not to make use of the thickness of the deposited lanthanum hydroxide layer, since it is driven by a complex diffusion-reaction problem. Figure 2b thus displays the relative reflectivity change $R-1$ under illumination at 490 nm as a function of the surface pH as computed using the model detailed in SI. The results are displayed in the $9.5 \leq pH \leq 11.5$ range for the sake of clarity. It is easily seen that the pH value at which the reflectivity starts to decrease is almost independent of the applied current density. We therefore conclude that the lanthanum hydroxide precipitation controls the measured reflectivity as described in Figure 1, and that the diffusion model in SI correctly describes the pH evolution at the electrode up to the precipitation threshold.

3.2 Metallic glass electrodes

3.2.1 Material's properties

The $Zr_{65}Ni_{35}$ binary metallic glass is a known HER catalyst[21] that can be processed using standard microfabrication techniques.[22] The obtained metallic glass thin films were checked to be amorphous and were extensively characterized (see SI). In particular, mechanical properties of the film were determined using nanoindentation. The Young's modulus is estimated to be 78 ± 8 GPa (see SI). The limit of the elastic regime is assumed to be attained when pop-in occurs, and the large number of indentation tests also allows to estimate the dispersion of the contact pressure at pop-in.

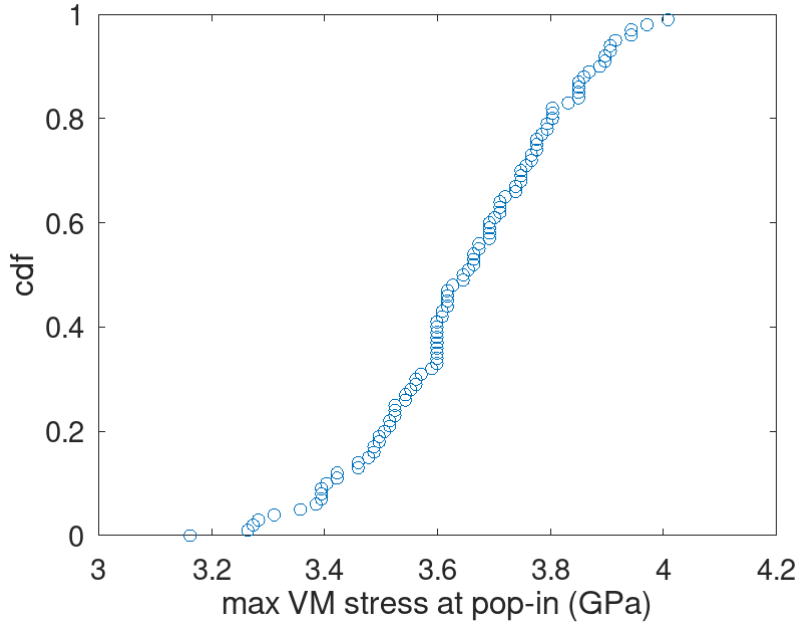


Figure 3: Cumulative density function of the maximum Von Mises stress under the indent at pop-in.

This is illustrated by Figure 3, which shows the cumulative density function of the maximum Von Mises stress under the indent at pop-in. Weibull's law is shown to correctly describe this dispersion, with a modulus of approximately 24, which is large enough to be considered almost deterministic (see SI). Keeping 3.6 GPa as the value of the Von Mises stress at pop-in initiation, the uniaxial yield strain is estimated to be more than 4.5%. This

quantifies the outstanding mechanical properties of the $Zr_{65}Ni_{35}$ film. The film also exhibits a low resistivity at room temperature (about 1.86 $\mu\Omega$.m), and has therefore been used as a cathode to produce hydrogen.

3.2.2 Reflectivity calibration for the $Zr_{65}Ni_{35}$ films

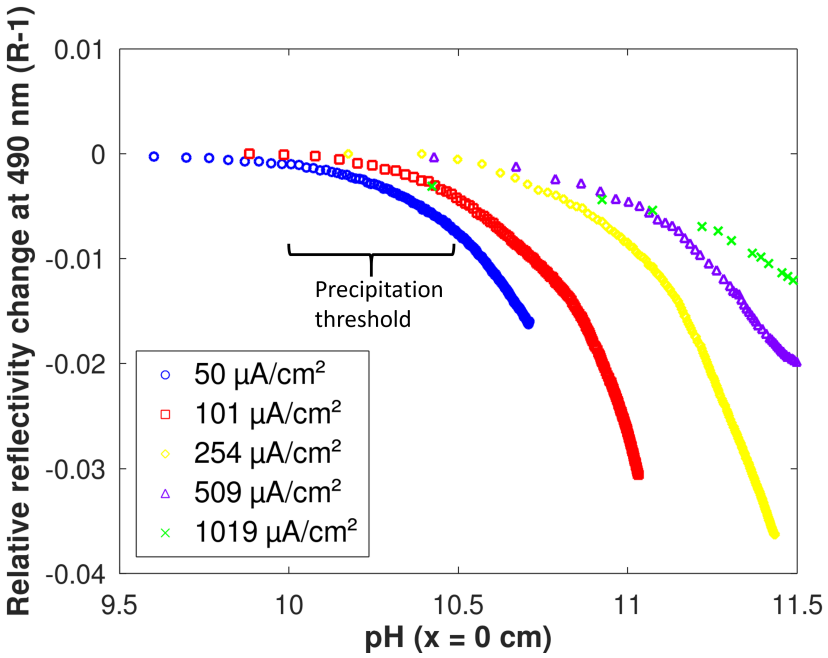


Figure 4: Relative reflectivity change at 490 nm as a function of the computed pH at the $Zr_{65}Ni_{35}$ electrode surface in a lanthanum hydroxide containing solution at pH=4.3.

Figure 4 displays the calibration curves obtained for the $Zr_{65}Ni_{35}$ electrode under the same conditions as those of Figure 2b. A very similar behavior is obtained, with a precipitation threshold almost independent of the applied current density. It is therefore concluded that the reflectivity of the $Zr_{65}Ni_{35}$ surface is also controlled by the precipitation of the lanthanum hydroxide, so that the time t_{pH} at which the reflectivity starts to decrease is an indicator of the local current density.

It should be highlighted that the diffusion model predicts that the maximum pH value is always obtained at the electrode surface. This ensures that the precipitation starts at the very electrode surface, so that the spatial resolution of the current density measurements is

that of the reflectivity measurements. It should also be noted that the model points to two adjustment parameters one could use to set, for a given current density, the time at which precipitation starts in a desired range : both the initial pH and the lanthanum hydroxide concentration could be used to accommodate varied experimental conditions.

3.3 Application to metallic glass cantilevers

The imaging technique reported herein was thus been applied to microcantilevers fabricated out of a 500 nm thick $Zr_{65}Ni_{35}$ layer (see SI), which were used as a cathode in chronopotentiometric water-splitting experiments. The electrolyte had a pH of .1 and a lanthanum hydroxide concentration of 1 mM. The cantilevers' reflectivity was computed along the experiment, using the first image as a reference. The sample being fixed and the additional experiments (not shown here) suggesting that the cantilevers do not deform during chronopotentiometric measurements, the reflectivity changes are ascribed to the lanthanum hydroxide precipitation, as in the reported calibration experiments.

Figure 5a displays a typical relative reflectivity change observed under 700 nm illumination on two adjacent cantilevers during chronopotentiometry (-78 μA.cm^{-2}). During this experiment, the cantilever on top was left free while the cantilever at the bottom of the image was bent away from the observed surface. The contrast map on the top cantilever clearly reveals that the hydrogen production is not uniform on the cantilever surface, thus highlighting the need, even in such a simple arrangement, to be able to monitor the local hydrogen production rate. According to the previous calibrations, this reflectivity map suggests that the production rate is much higher near the cantilever tip, and this may be a consequence of both the initial stresses in the cantilever resulting from the fabrication process (see SI) and the geometry. The previous calibrations could be used to retrieve the local current density. This requires to extract the time t_{pH} at which, for each pixel, the lanthanum hydroxide precipitation starts. This time was computed from the recorded images using an algorithm

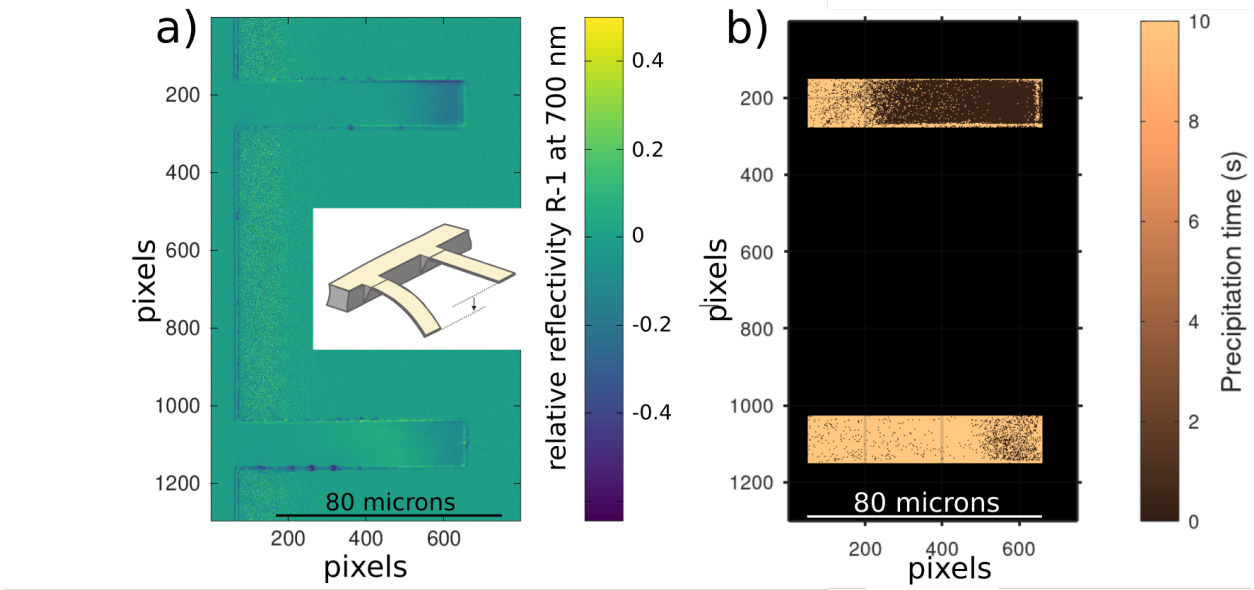


Figure 5: a) Relative reflectivity change at 700 nm for two adjacent cantilevers (unitless), the bottom one being bent down (away from the microscope objective) by 2.9 μm. It was obtained after 50 s of chrono-potentiometric measurements at -78 μA.cm^{-2} in a lanthanum hydroxide containing solution at pH = 3.1. b) Map of the time t_{pH} at which the precipitation starts.

described in SI and is displayed in Figure 5b. It should be recalled that the calibration procedure proposed in Section 3.2.2, which aims at establishing the correspondence between t_{pH} and the local H_2 production rate, essentially assumes a one-dimensional diffusion problem, normal to the electrode's surface. However, the large in-plane reflectivity gradients call for a 3D diffusion problem, which is out of the scope of the present letter, to relate the local current density to t_{pH}.

The role of the mechanical state is further illustrated by considering the cantilever at the bottom of the image. It is bent down so that the observed surface experiences an additional, non-uniform, tensile strain, and the deformed cantilever is almost aligned with the substrate (the total elastic strain at the cantilever's surface thus vanishes). The corresponding displacement field may be estimated from beam theory, and reads as a third-order polynomial in the distance from the cantilever base. The strain field being essentially symmetric within a cross-section, the exposed electrode area is not altered by the mechanical loading. It is clearly seen that the reflectivity change is significantly altered, suggesting that the hydrogen production is drastically reduced at this tensile surface. This is further illustrated by the precipitation time map : precipitation only occurs at the very tip of the cantilever. This provides a direct visualization of the effect of strain on the electrocatalytic behavior of the considered material. This result is qualitatively in line with the literature[1–7] on crystalline materials, which suggests that the mechanical state can significantly modify the electrocatalytic behavior of metals. The above result experimentally supports the conclusion that amorphous metals may be promising candidates for strain-engineered electrocatalysts,[23] especially considering their large elastic regime.

Conversely, Figure 6 displays similar images obtained when the cantilever at the bottom of the image was bent upwards (towards the microscope objective) by 11.3 μm. The observed surface thus experiences compression. Whereas the undeformed cantilever displays a reflectivity decrease only over a small area near the cantilever tip after 50 s, the bent cantilever displays a significant reflectivity decrease across its entire surface, suggesting that the hydro-

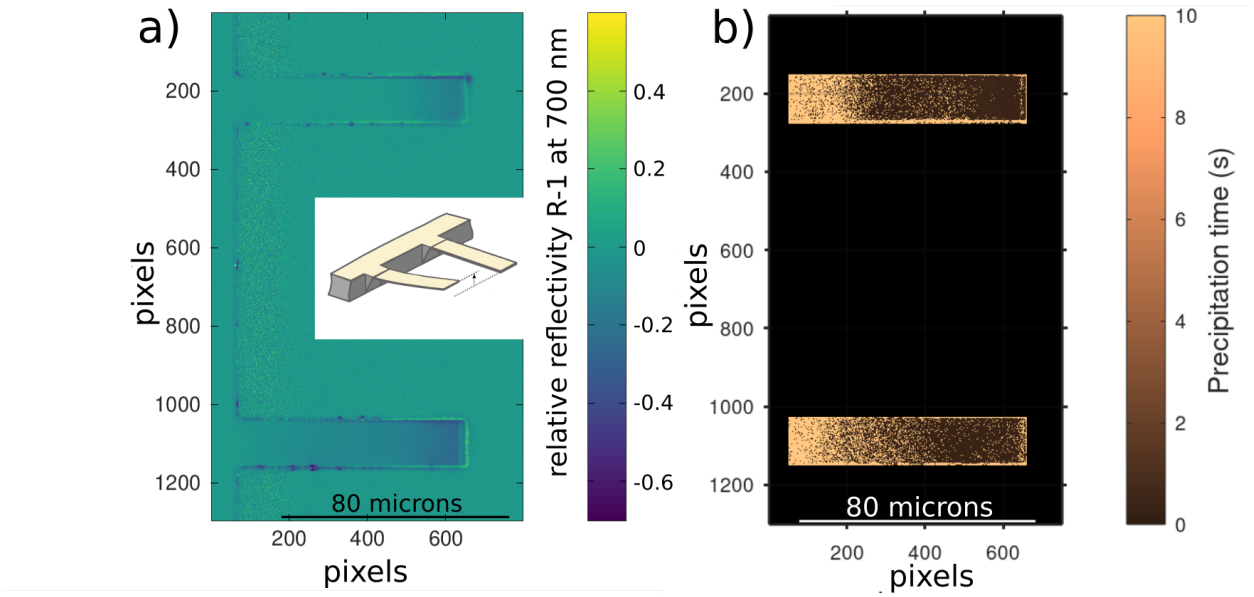


Figure 6: a) Relative reflectivity change at 700 nm for two adjacent cantilevers (unitless), the bottom one being bent upwards (towards the microscope objective) by 11.3 μm. It was obtained after 50 s of chrono-potentiometric measurements at -78 μA.cm^{-2} in a lanthanum hydroxide containing solution (1 mM) at pH = 3.1. b) Map of the time t_{pH} at which the precipitation starts.

gen production is much more intense under this mechanical loading (Figure 6a). However, this may be misleading, as indicated by the precipitation time map Figure 6b, which shows almost similar precipitation times for the two cantilevers. As demonstrated with the calibrations above, the latter quantity should be considered instead of the raw relative reflectivity change.

These findings further suggest that the mechanical quantity of interest may be more complex than simple uniaxial strain. According to beam theory, uniaxial strain varies linearly with distance from the contact point when the cantilever is deflected. However, the observed change in reactivity remains minimal near the cantilever's fixed end in Figures 5 and 6. This demonstrates how the proposed setup, combined with a tailored inverse problem approach, could be used to determine the optimal strain state.

4 Conclusions

This study demonstrates the potential of the proposed imaging setup to reveal non-uniform hydrogen production, regardless of its origin —whether geometrical, defect-related, or otherwise. Accessible and versatile, this method enables measurements at any optically accessible scale, thus providing an unprecedented experimental bridge between DFT results and classical electrochemical measurements at the electrode scale. Its key strength lies in its ease of implementation, which allows monitoring of hydrogen production on deformable structures. This approach paves the way for a general methodology to investigate the impact of complex strain states on the electrocatalytic performance of materials. In this study, the set-up enabled the evaluation —in a single experiment— of the effects of varied mechanical conditions on electrocatalytic activity. Notably, the results highlight the critical role of the mechanical state in modulating the performance of the considered amorphous metal. By subjecting the material to different strain conditions, significant variations of its electrocatalytic efficiency

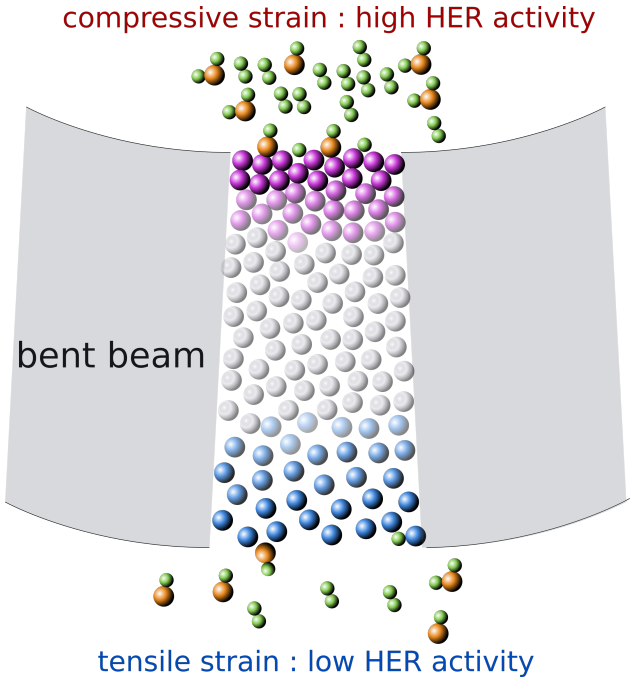


Figure 7: Schematic view of the reported findings. For the considered amorphous metal, the surface experiencing compression is more active for HER than the surface under tensile strain.

were observed, suggesting that mechanical deformation can either enhance or inhibit hydrogen evolution reactions, depending on the applied strain (see Figure 7). This insight is particularly valuable for designing materials with tailored mechanical and catalytic properties, as it underscores the interplay between structural flexibility and catalytic performance. These findings underscore the method's potential to revolutionize the analysis of electrocatalytic materials under mechanical strain, and in particular to enable the development of amorphous metal electrodes.

Acknowledgement

This work was supported by the French RENATECH network and its FEMTO-ST technological facility. It has also benefited from the support of IRT-M2P (H2-Elyse), from EIPHI Graduate School (contract "ANR-17-EURE-0002"), and from CNRS through the PEPS and 80prime programs. The support of the AMETISTE platform is also acknowledged.

Supporting Information Available

The following file is available free of charge.

- `SI_common.pdf` : Details about the amorphous metal deposition, characterization, and processing ; pH calculation at the electrode (PDF).

References

(1) Mavrikakis, M.; Hammer, B.; Nørskov, J. K. Effect of Strain on the Reactivity of Metal Surfaces. *Phys. Rev. Lett.* **1998**, *81*, 2819–2822.

(2) Martínez-Alonso, C.; Guevara-Vela, J. M.; LLorca, J. Understanding the effect of me-

chanical strains on the catalytic activity of transition metals. *Phys. Chem. Chem. Phys.* **2022**, *24*, 4832–4842.

(3) Kibler, L. A.; El-Aziz, A. M.; Hoyer, R.; Kolb, D. M. Tuning Reaction Rates by Lateral Strain in a Palladium Monolayer. *Angewandte Chemie International Edition* **2005**, *44*, 2080–2084.

(4) Strasser, P.; Koh, S.; Anniyev, T.; Greeley, J.; More, K.; Yu, C.; Liu, Z.; Kaya, S.; Nordlund, D.; Ogasawara, H.; Toney, M. F.; Nilsson, A. Lattice-strain control of the activity in dealloyed core–shell fuel cell catalysts. *Nature Chemistry* **2010**, *2*, 454–460.

(5) Wu, G.; Han, X.; Cai, J.; Yin, P.; Cui, P.; Zheng, X.; Li, H.; Chen, C.; Wang, G.; Hong, X. In-plane strain engineering in ultrathin noble metal nanosheets boosts the intrinsic electrocatalytic hydrogen evolution activity. *Nature Communications* **2022**, *13*, 4200.

(6) Redondo, J.; Subbian, J.; Monclús, M.; Pendashteh, A.; Pérez, D.; Mehdi, M.; Ruiz-Hervías, J.; Molina Aldareguia, J.; LLorca, J. Effect of elastic strains on the electrocatalytic activity of Au thin films for the hydrogen evolution reaction. *Journal of Catalysis* **2025**, *447*, 116151.

(7) Redondo, J.; Subbian, J.; Monclus, M. A.; Vassilev-Galindo, V.; Molina-Aldareguia, J. M.; LLorca, J. Modulating the Electrocatalytic Activity of Intermetallic Compounds for the Hydrogen Evolution Reaction via Elastic Strain Engineering. *ACS Catalysis* **2025**, *15*, 20216–20229.

(8) Yang, X.; Wang, Y.; Tong, X.; Yang, N. Strain Engineering in Electrocatalysts: Fundamentals, Progress, and Perspectives. *Advanced Energy Materials* **2022**, *12*, 2102261.

(9) Yoon, C.; Cocke, D. L. Potential of amorphous materials as catalysts. *Journal of Non-Crystalline Solids* **1986**, *79*, 217–245.

(10) Guo, T.; Li, L.; Wang, Z. Recent Development and Future Perspectives of Amorphous Transition Metal-Based Electrocatalysts for Oxygen Evolution Reaction. *Advanced Energy Materials* **2022**, *12*, 2200827.

(11) Jia, B.; Liu, G.; Zhang, B.; Zheng, J.; Yin, K.; Lin, J.; Han, C.; Fan, X.; Xu, M.; Ye, L. General Modification Strategy on Amorphous Materials to Boost Catalytic Performance. *Advanced Functional Materials* **2024**, *34*, 2405867.

(12) Ling, T.; Yan, D.-Y.; Wang, H.; Jiao, Y.; Hu, Z.; Zheng, Y.; Zheng, L.; Mao, J.; Liu, H.; Du, X.-W.; Jaroniec, M.; Qiao, S.-Z. Activating cobalt(II) oxide nanorods for efficient electrocatalysis by strain engineering. *Nature Communications* **2017**, *8*, 1509.

(13) Fan, C.; Wan, Z.; Pan, M.; Hou, J.; Shi, Y.; Guo, W.; Wang, G.; Peng, S.; Jing, Q.; Chen, L. Photoassisted Electrochemical Hydrogen Evolution Reaction of MFe2O4@Ultrathin Black Phosphorus Amorphous–Crystalline Interface. *ACS Applied Materials & Interfaces* **2022**, *14*, 54748–54757, PMID: 36458335.

(14) Gu, Z.; Zhang, Y.; Wei, X.; Duan, Z.; Ren, L.; Ji, J.; Zhang, X.; Zhang, Y.; Gong, Q.; Wu, H.; Luo, K. Unveiling the Accelerated Water Electrolysis Kinetics of Heterostructural Iron-Cobalt-Nickel Sulfides by Probing into Crystalline/Amorphous Interfaces in Stepwise Catalytic Reactions. *Advanced Science* **2022**, *9*, 2201903.

(15) Liu, Y.; Sakthivel, T.; Hu, F.; Tian, Y.; Wu, D.; Ang, E. H.; Liu, H.; Guo, S.; Peng, S.; Dai, Z. Enhancing the d/p-Band Center Proximity with Amorphous-Crystalline Interface Coupling for Boosted pH-Robust Water Electrolysis. *Advanced Energy Materials* **2023**, *13*, 2203797.

(16) Wang, M.; Feng, X.; Li, S.; Ma, Y.; Peng, Y.; Yang, S.; Liu, Y.; Lei, H.; Dang, J.; Zhang, W.; Cao, R.; Zheng, H. Spinel-Type Metal Oxides with Tailored Amorphous/Crystalline Heterointerfaces for Enhanced Electrocatalytic Water Splitting. *Advanced Functional Materials* **2024**, *34*, 2410439.

(17) Liu, G.-Q.; Zhang, Y.-D.; Zhang, X.-L.; Wang, C.-G.; Li, Y.; Wu, L.; Gu, C.; Zheng, X.-S.; Gao, M.-R.; Yu, S.-H. Amorphous/Crystalline Heterojunction Engineered High-Density Strain in RuSeTe for Efficient Alkaline Hydrogen Evolution Reaction. *Advanced Materials* **2026**, *38*, e17922.

(18) Oliver, W. C.; Pharr, G. M. An improved technique for determining hardness and elastic modulus using load and displacement sensing indentation experiments. *Journal of Materials Research* **1992**, *7*, 1564–1583.

(19) Leipner, H.; Lorenz, D.; Zeckzer, A.; Lei, H.; Grau, P. Nanoindentation pop-in effect in semiconductors. *Physica B: Condensed Matter* **2001**, *308-310*, 446–449, International Conference on Defects in Semiconductors.

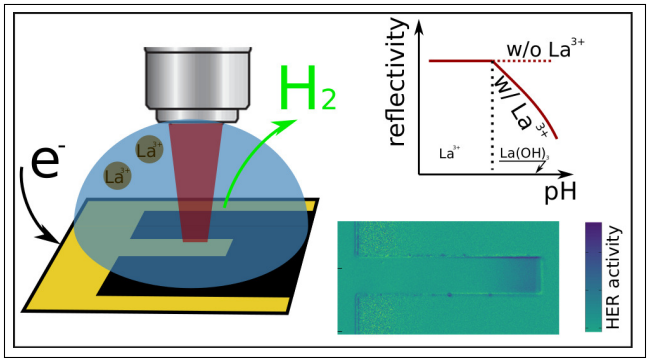
(20) Lorenz, D.; Zeckzer, A.; Hilpert, U.; Grau, P.; Johansen, H.; Leipner, H. S. Pop-in effect as homogeneous nucleation of dislocations during nanoindentation. *Phys. Rev. B* **2003**, *67*, 172101.

(21) Mihailov, L.; Spassov, T.; Bojinov, M. Effect of microstructure on the electrocatalytic activity for hydrogen evolution of amorphous and nanocrystalline Zr–Ni alloys. *International Journal of Hydrogen Energy* **2012**, *37*, 10499–10506.

(22) Volland, A. Etude des effets d'échelle sur le comportement mécanique de film mince en verre métallique. Thesis, Université de Grenoble, 2012.

(23) Yao, Q.; Yu, Z.; Li, L.; Huang, X. Strain and Surface Engineering of Multicomponent Metallic Nanomaterials with Unconventional Phases. *Chemical Reviews* **2023**, *123*, 9676–9717, PMID: 37428987.

TOC Graphic


H2
e-
La3+
La3+
reflectivity
w/o La3+
w/ La3+
La3+
La(OH)3
pH
HER activity